IOP Publishing Journal of Geophysics and Engineering
J. Geophys. Eng. 14 (2017) 811–821 (11pp) https://doi.org/10.1088/1742-2140/aa6e7a

# Two modified symplectic partitioned Runge–Kutta methods for solving the elastic wave equation

**Bo Su[1,2], Xianguo Tuo[3] and Ling Xu[4,5]**

[1] Graduate School, China Academy of Engineering Physics, Mianyang, Sichuan 621900, People's Republic of China
[2] School of Computer Science and Technology, Southwest University of Science and Technology, Mianyang 621010, People's Republic of China
[3] Key Subject Lab of National Defense for Nuclear Waste and Environmental Safety, Southwest University of Science and Technology, Mianyang 621010, People's Republic of China
[4] School of Human Settlements and Civil Engineering, Xi'an Jiaotong University, Xi'an, Shaanxi 710049, People's Republic of China

E-mail: suyu820@163.com

Received 17 October 2016, revised 27 March 2017
Accepted for publication 21 April 2017
Published 13 June 2017

**Abstract**

Based on a modified strategy, two modified symplectic partitioned Runge–Kutta (PRK) methods are proposed for the temporal discretization of the elastic wave equation. The two symplectic schemes are similar in form but are different in nature. After the spatial discretization of the elastic wave equation, the ordinary Hamiltonian formulation for the elastic wave equation is presented. The PRK scheme is then applied for time integration. An additional term associated with spatial discretization is inserted into the different stages of the PRK scheme. Theoretical analyses are conducted to evaluate the numerical dispersion and stability of the two novel PRK methods. A finite difference method is used to approximate the spatial derivatives since the two schemes are independent of the spatial discretization technique used. The numerical solutions computed by the two new schemes are compared with those computed by a conventional symplectic PRK. The numerical results, which verify the new method, are superior to those generated by traditional conventional methods in seismic wave modeling.

Keywords: elastic wave equation, modified symplectic scheme, partitioned Runge–Kutta method, finite difference method

(Some figures may appear in colour only in the online journal)

## 1. Introduction

Numerically solving the seismic wave equation is a fundamental development for wave-equation-based imaging methods (Whitmore and Lines 1986). Direct numerical schemes for solving the elastic wave equation involve the discretizations of both spatial and temporal derivatives. Spatial derivatives have been explored extensively, of which the most popular and widely used methods are finite difference methods (FDM) (Alford *et al* 1974, Dablain 1986, Moczo 1989). There are other popular direct methods for spatial discretization, such as the pseudo-spectral method (Kosloff and Baysal 1982), the finite element method (FEM) (Marfurt 1984) and the spectral element method (SEM) (Patera 1984, Komatitsch and Vilotte 1998). Each method is characterized by its own merits and shortcomings.

Compared with spatial discretization, temporal discretization has been investigated far less substantially (Chen 2007, Liu *et al* 2015a). We accordingly concentrate on the wave equation's temporal discretization in this study. Numerical schemes for temporal derivatives additionally involve a so-called time-dispersion error (Wang and Xu 2015,

[5] Author to whom any correspondence should be addressed.

 

Liu *et al* 2017a, 2017b). The second-order central difference method (CDM) (Virieux 1984, 1986) and the explicit Newmark scheme (Liu *et al* 2014a) have been widely used in the numerical computing field due to their simplicity. However, a main drawback of both the CDM and Newmark scheme is their serious numerical dispersion (Liu *et al* 2015a) due to their low numerical order. To reduce the numerical dispersion error, a small temporal time interval should be used (Ma *et al* 2014). However, a small temporal interval would lead to a proportional increase of the computational cost. A natural technique with which to increase computational efficiency is the use of higher-order schemes. Chen (2007) presented three methods for high-order temporal discretization: the fourth-order Lax–Wendroff method (LWM), the fourth-order Nyström method, and the splitting method. The LWM uses high-order spatial derivatives to correct the temporal accuracy. A fourth-order LWM is generally adopted for its strong stability and easy implemenation, although an arbitrary even order can be obtained by the LWM (Dablain 1986, De Basabe and Sen 2010). Nyström methods are designed to solve a second-order temporal derivative dynamic system (Okunbor and Skeel 1994). The Splitting methods apply two Runge–Kutta methods to solve the reduced-order system (Liu *et al* 2017a). Li *et al* (2011, 2012) introduced a third-order symplectic partitioned Runge–Kutta (TPRK) scheme to solve elastic wave equations, wherein the discrete singular convolution differentiator was used for spatial discretization. The computational cost of the TPRK method may be moderate when solving acoustic and elastic wave equation because TPRK requires three times the numerical evaluation of spatial derivatives (Li *et al* 2011). The symplecticity is an intrinsic structure of Hamiltonian dynamics (Feng and Qin 2010), and wave propagation in non-dissipative media can be evaluated in a Hamiltonian (H) framework. A numerical method that preserves this symplecticity is called a symplectic scheme (Chen 2007, 2009, Feng and Qin 2010, Li *et al* 2011, 2012). Preserving the symplectic structure of the seismic wave equation may be very suitable for large-scale and long-term wave phenomenon investigations (Li *et al* 2012). Previous studies have ensured that high-order, such as fourth-order, symplectic techniques are available for seismic wave equations. However, higher-order schemes generally necessitate more than three times the numerical evaluation of spatial derivatives in each time step, and these computational costs may be unfeasible for large-scale models or computation-intensive imaging methods.

Ma *et al* (2014) provided a detailed discussion regarding second- to fourth-order symplectic schemes for acoustic and elastic wave simulations. These schemes were combined with nearly analytic discrete (Yang *et al* 2003, 2007) operators. Through theoretical analyses and numerical simulations, they concluded that the second-order PRK (SPRK) is suitable for wavefield simulations because of its high-efficiency, which only involves two times the numerical evaluation of spatial derivatives in each time step. Unfortunately, the SPRK is not capable of effectively suppressing temporal dispersion (Liu *et al* 2017a). Accordingly, third-order symplectic schemes are a compromise between computational costs and numerical accuracy (Liu *et al* 2015a, 2017a, 2017b). In this work, the modified strategy proposed by Liu *et al* (2015a, 2017a, 2017b) is adopted to construct two modified third-order symplectic PRK methods. By including additional terms into the two-stage second-order Runge–Kutta–Nyström (RKN) (Feng and Qin 2010), these two third-order modified symplectic schemes can be derived, which will represent a reduction of one intermediate time step compared with conventional third-order sympelctic methods. The symplectic coefficients of the two new methods are determined by a Taylor series expansion. Interestingly, the two methods possess the same coefficients, while their numerical stability and dispersion properties are quite different. The two symplectic schemes are independent of the spatial approximation operator used, and the FDM is used for the ease of discussion. Two numerical experiments are subsequently conducted to verify the validity of the proposed method for seismic wave modeling.

## 2. Two modified symplectic PRK methods

To construct a symplectic scheme, the fundamental issue is to reformulate the dynamic system into a Hamiltonian system. We consider the following elastic wave equation (Aik and Richards 1980):H

$$\begin{cases} \rho\dfrac{\partial^2 u_i}{\partial t^2} = \dfrac{\partial \sigma_{ij}}{\partial x_j} + f_i \\ \sigma_{ij} = c_{ijkl}\varepsilon_{kl} \\ \varepsilon_{kl} = \dfrac{1}{2}\left(\dfrac{\partial u_k}{\partial x_l} + \dfrac{\partial u_l}{\partial x_k}\right) \end{cases}, \tag{1}$$

where $i, j, k, l = 1, 2, 3$; $u_i$ is the displacement component; $\rho(x, y, z)$ is the mass density; $x_j$ is the Cartesian coordinate; $\sigma_{ij}$ is the stress tensor; $f_i$ denotes the force-source term; $c_{ijkl}$ are the elastic constants; and $\varepsilon_{kl}$ is the strain tensor. By defining the velocity variable $v_i = \dfrac{\partial u_i}{\partial t}$, the displacement vector can be written as $U = (u_1, u_2, u_3)^T$, and the velocity vector can be written as $V = (v_1, v_2, v_3)^T$, respectively. Let $\Omega$ be a domain in the Euclidean space $R^d$, and let $H(\boldsymbol{U}, \boldsymbol{V}) = \dfrac{1}{2}\iiint_\Omega \left(\boldsymbol{V}^T \cdot \boldsymbol{V} + \dfrac{1}{\rho}\sigma_{ij}\varepsilon_{ij}\right)\mathrm{d}\Omega$ be a sufficiently smooth real function defined on $\Omega$, from which we can obtain the following Hamiltonian system:

$$\begin{cases} \dot{U} = \dfrac{\partial H(U, V)}{\partial V} \\ \dot{V} = -\dfrac{\partial H(U, V)}{\partial U} \end{cases}. \tag{2}$$

The application of two-stage Runge–Kutta methods (Okunbor and Skeel 1992) to equation (2) leads to the following numerical system:

$$\begin{cases} V_i = V^n + \Delta t\sum_{j=1}^{s} a_{ij} L U_j \\ U_i = U^n + \Delta t\sum_{j=1}^{s} A_{ij} V_j \\ V^{n+1} = V^n + \Delta t\sum_{i=1}^{s} b_i L U_i \\ U^{n+1} = U^n + \Delta t\sum_{i=1}^{s} B_i V_i \end{cases} \quad i = 1,\cdots,s, \tag{3}$$

where $\Delta t$ is the time increment; $L$ is the FD operator matrix for the spatial differential, the symmetry of which is discussed by Liu *et al* (2017a); and $a_{ij}$, $A_{ij}$, $b_i$ and $B_i$ are symplectic coefficients that must be defined. To preserve the symplecticity, equation (3) should satisfy the following condition (Feng and Qin 2010):

$$\mathrm{d}V_{n+1} \wedge \mathrm{d}U_{n+1} = \mathrm{d}V_n \wedge \mathrm{d}U_n, \tag{4}$$

where $\wedge$ denotes the wedge product. If scheme (3) satisfies equation (4), the standard symplectic structure is preserved (Feng and Qin 2010). Using equation (4), Sun (1993) proved that the symplectic condition for scheme (3) can be expressed as:

$$b_i A_{ij} + B_h a_{ji} - b_i B_j = 0 \quad i, j = 1,\cdots,s. \tag{5}$$

From scheme (3) and equation (5), we can obtain a two-stage explicit PRK method with a second-order time integrator (Ma *et al* 2014):

$$\begin{aligned} U_1 &= U^n + \Delta t B_1 V^n \quad V_1 = V^n + \Delta t b_1 L U_1 \\ U^{n+1} &= U_1 + \Delta t B_2 V_1 \quad V^{n+1} = V_1 + \Delta t b_2 L U^{n+1}, \end{aligned} \tag{6}$$

where

$$B1 = 0, \quad B2 = 1, \quad b1 = b2 = 1/2, \tag{7a}$$

or

$$B1 = B2 = 1/2, \quad b1 = 1, \quad b2 = 0. \tag{7b}$$

The parameters in (7*a*) require the computation of the spatial derivatives twice, while group (7*b*) only requires this computation once. A symplectic scheme with the parameters in (7*a*) for the seismic wave equation is more stable and accurate than a symplectic scheme with the parameters in (7*b*). Accounting for third- or fourth-order schemes necessitates the computation of the spatial derivatives three or four times. Hence, the parameters in (7*a*) are commonly used for wavefield simulations in consideration of computational efficiency.

To improve the accuracy of the second-order symplectic PRK, Mclachlan and Atela (1992) presented a scheme using the minimal truncation error principle, while Liu *et al* (2015a, 2015b) utilized the minimal frequency error principle. Nevertheless, the accuracy of the optimized schemes are still far less than that of the third-order symplectic scheme (Liu *et al* 2014a). Based on the modified strategy proposed by Liu *et al* (2015a, 2017a, 2017b), we develop two efficient schemes by including additional terms into system (6). One scheme is to add $LV^n$ into the first equation of scheme (6) to generate a new method for a higher-order symplectic PRK. For comparison purposes, we denote this scheme as method 1 (M1):

$$\begin{aligned} U_1 &= U^n + \Delta t B_1 V^n + \Delta t^3 B_3 L V^n \quad V_1 = V^n + \Delta t b_1 L U_1 \\ U^{n+1} &= U_1 + \Delta t B_2 V_1 \quad V^{n+1} = V_1 + \Delta t b_2 L U^{n+1}. \end{aligned} \tag{8}$$

The new term $LV^n$ is used to modify the accuracy of scheme (6), following which the accuracy changes from that of second-order to third-order. Based on the truncated Taylor series expansion, we can obtain third-order symplectic conditions. The detailed derivation is presented in appendix A, and the order condition is as follows:

$$\begin{cases} b_1 + b_2 = 1 \\ B_1 + B_2 = 1 \\ b_2 + b_1 B_1 = \dfrac{1}{2} \\ b_1 b_2 B_2 = \dfrac{1}{6} \\ b_1 B_1 B_2 + B_3 = \dfrac{1}{6} \end{cases}. \tag{9}$$

The solution of (9) is:

$$b_1 = \frac{2}{3}, \quad b_2 = \frac{1}{3}, \quad B_1 = \frac{1}{4}, \quad B_2 = \frac{3}{4}, \quad B_3 = \frac{1}{24}. \tag{10}$$

Equation (8) with the coefficients in (10) is known as symplecticity (see appendix B). Another modified PRK method can be obtained by adding $LV_1$ to the third equation of equation (6), which is denoted as M2. M2 can be written in the following form:

$$\begin{aligned} U_1 &= U^n + \Delta t B_1 V^n \quad V_1 = V^n + \Delta t b_1 L U_1 \\ U^{n+1} &= U_1 + \Delta t B_2 V_1 + \Delta t^3 B_3 L V_1 \quad V^{n+1} = V_1 + \Delta t b_2 L U^{n+1}. \end{aligned} \tag{11}$$

Interestingly, the form of scheme M1 is slightly different from the form of scheme M2, but schemes M1 and M2 have the same symplectic coefficients. As discussed in the next section, the stability and dispersion of schemes M1 and M2 are different, although they have the same coefficients, and thus they can be used in different situations. One can obtain other modified schemes if high-order terms are added into the second equation of scheme (6). Here, we generate two modified symplectic PRK schemes based on a two-stage explicit PRK. It should be noted that, if an additional item is added into a three- or four-stage explicit PRK, we could produce a series of modified schemes, which will be discussed in further research.

## 3. Stability and dispersion analysis

Stability is very important for numerical calculations and time increments should be bounded by stability conditions (Liu *et al* 2015c). Numerical results are fundamentally affected by numerical dispersion. In this section, we present a theoretical analysis concerning these two schemes. For comparison purposes, three alternative methods are adopted, namely, the SPRK scheme (Ma *et al* 2014), third-order PRK (TPRK) scheme (Iwatsu 2009, Li *et al* 2012) and fourth-order RKN (TRKN) scheme (Chen 2007).

### 3.1. Stability conditions

Let the harmonic solution on the $n$th time layer at the grid point $(x, y, z)$ be written as follows:

$$\begin{pmatrix} V^{\mathrm{n}} \\ U^{\mathrm{n}} \end{pmatrix} = \begin{pmatrix} V_x \\ V_y \\ V_z \\ U_x \\ U_y \\ U_z \end{pmatrix} \exp(\mathrm{i}(\omega_{\mathrm{num}}\mathrm{n}\Delta t - k_x x - k_y y - k_z z)), \quad (12)$$

where $\Delta t$ is the time increment; $\omega_{\mathrm{num}}$ is the frequency; $k_x = k \sin\theta \cos\varphi$, $k_y = k \sin\theta \sin\varphi$ and $k_z = k \cos\theta$; and $\mathbf{k} = (k_x, k_y, k_z)$ is the wavenumber vector.

Substituting the harmonic solution (12) into equations (8) and (11), respectively, we retrieve the form $(V^{n+1}\ U^{n+1})^T = G(V^n\ U^n)^T$, in which $G$ is the growth matrix. If $\psi$ represents the eigenvalue of $G$ and $\lambda$ denotes the eigenvalue of $L$, we have the following characteristic polynomials of $G$:

$$f(\psi) = \prod_{i=1}^{3}\left(\psi^2 - \left(2 + \Delta t^2\lambda_i + \frac{1}{12}\Delta t^4\lambda_i^2 + \frac{1}{144}\Delta t^6\lambda_i^3\right)\psi + 1\right), \quad (13)$$

and

$$f(\psi) = \prod_{i=1}^{3}\left(\psi^2 - \left(2 + \Delta t^2\lambda_i + \frac{1}{12}\Delta t^4\lambda_i^2 + \frac{1}{432}\Delta t^4\lambda_i^3\right)\psi + 1\right). \quad (14)$$

Equations (13) and (14) correspond to M1 and M2, respectively. To maintain the stability of M1 and M2, the eigenvalue of $G$ should satisfy $|\psi| \leqslant 1$ (De Basabe and Sen 2007). From equations (13) and (14), the stability condition can be correspondingly converted to

$$\left|2 + \Delta t^2\lambda_i + \frac{1}{12}\Delta t^4\lambda_i^2 + \frac{1}{144}\Delta t^6\lambda_i^3\right| \leqslant 2 \Leftrightarrow -5.308 \leqslant \Delta t^2\lambda_i \leqslant 0, \quad (15)$$

**Table 1.** Stability parameters for solving the elastic wave equation.

| | Method | | | | |
|---|---|---|---|---|---|
| Stability parameters | M1 | M2 | SPRK | TPRK | TRKN |
| $\lvert\Delta t^2\lambda_i\rvert_{\max}$ | 5.308 | 12 | 4 | 7.107 | 6.69 |
| $a$ | 0.4476 | 0.4469 | 0.4446 | 0.4429 | 0.4467 |
| $b$ | 0.838 | 1.2599 | 0.7274 | 0.9695 | 0.9407 |

and

$$\left|2 + \Delta t^2\lambda_i + \frac{1}{12}\Delta t^4\lambda_i^2 + \frac{1}{432}\Delta t^6\lambda_i^3\right| \leqslant 2 \Leftrightarrow -12 \leqslant \Delta t^2\lambda_i \leqslant 0. \quad (16)$$

As observed from equation (1), the expression $\Delta t^2\lambda_i$ within equations (15) and (16) is related to $\lambda$, $\mu$ and $\rho$. From the discussion of Liu *et al* (2015a), we have the following relation:

$$\frac{\Delta t^2}{h^2}\left(a_1\frac{(\lambda + 2\mu)}{\rho} + a_2\frac{\mu}{\rho}\right) \leqslant |\Delta t^2\lambda_i|_{\max}. \quad (17)$$

From equation (15), we obtain

$$\frac{\Delta t^2}{h^2}\left(a_1\frac{(\lambda + 2\mu)}{\rho} + a_2\frac{\mu}{\rho}\right) \leqslant 5.308. \quad (18)$$

The simple form of equation (18) is represented by

$$\frac{\Delta t V_P}{h}\sqrt{1 + \frac{a}{r^2}} \leqslant b, \quad (19)$$

where $V_P$ is the $P$-wave velocity; $h$ is the spatial increment; $a = a_2/a_1$ and $b = \sqrt{5.308/a_1}$ are coefficients that need to be determined; and $r = V_P/V_S$ is the ratio of the $P$- and $S$- wave velocities. In table 1, the stability parameters for the 2D elastic wave equation are listed. M1, M2 and the three alternative methods are applied for time integration, and an eighth-order central FD operator is adopted for spatial approximation.

As is apparent from table 1, the largest value for the stability condition is observed for M2, while the smallest is derived from SPRK. The stability condition of TPRK is larger than that of TRKN, while they are both larger than that of M1. The values of $a$ are determined by the spatial FD operator and are almost equivalent, which means $r$ has nearly the same impact on the stability conditions of the five methods. The values of $b$ are substantially different, wherein the largest $b$ value corresponds to M2. This suggests that the time-step of M2 can vary in the largest range. The smallest $b$ value corresponds to SPRK. Compared with M2, the stability range of SPRK is reduced by 42.27%. TPRK and TRKN have almost the same stability range, both of which are larger than that of M1.

From the above discussion, an interesting phenomenon to note is that both M1 and M2 possess the same coefficients, but the stability range of M1 is 33.49% less than that of M2.

### *3.2. Numerical dispersion analysis*

Numerical dispersion is a major abstract artifact caused by the discretization of the wave equation (Yang 2006), which affects the reliability of the simulation results. Following the dispersion analysis developed by Moczo *et al* (2000), the dispersion ratio of the numerical velocity $V_{\text{num}}$ to the phase velocity $V_0$ is as follows:

$$R = \frac{V_{\text{num}}}{V_0} = \frac{\omega_{\text{num}}\Delta t}{2\pi S_p \alpha} = \frac{\text{Arc}\cos(\text{Re}(\lambda_i))}{2\pi S_p \alpha}, \tag{20}$$

where $\alpha = \dfrac{V_p \Delta t}{h}$ is the Courant number; $S_p = \dfrac{h}{\lambda}$ is the sampling ratio, where $\lambda$ denotes the wavelength; and $\lambda_i$ is the eigenvalue of the growth matrix $G$.

From equations (13) and (20), the dispersion ratio of M1 is written as:

$$R = \frac{\text{Arc}\cos\left(1 + \frac{1}{2}\Delta t^2\lambda_i + \frac{1}{24}\Delta t^4\lambda_i^2 + \frac{1}{288}\Delta t^6\lambda_i^3\right)}{2\pi S_p \alpha}. \tag{21}$$

Similarly, the dispersion ratio $R$ for M2 can be derived as:

$$R = \frac{\text{Arc}\cos\left(1 + \frac{1}{2}\alpha^2\gamma_i + \frac{1}{24}\alpha^4{\gamma_i}^2 + \frac{1}{864}\alpha^6{\gamma_i}^3\right)}{2\pi S_p \alpha}. \tag{22}$$

The anisotropic numerical dispersion curves of the five methods with eight-order FD operators are shown in figure 1. The angle of the wave propagation direction varies from 0° to 360°. Figure 1(a) demonstrates an $S_p = 0.4$ and (b) $S_p = 0.5$ with a small Courant number (time increment) of $\alpha = 0.2$. Meanwhile, figure 1(c) shows an $S_p = 0.4$ and (d) $S_p = 0.5$ with a relatively larger Courant number of $\alpha = 0.4$. Comparing the dispersion curves in these plots, we can see that, for the same propagation angle (except for the $x$- and $z$-directions), the dispersion error of SPRK is larger than those of the other four schemes. The dispersion curves of M1, M2, TPRK and TRKN overlap with each other, and it is thus difficult to distinguish the differences among these methods. With a small Courant number of $\alpha = 0.2$, the dispersion curve of TRKN, which displays the lowest dispersion, obviously separates from those of M1, M2 and TPRK. Generally, M1, M2 and TPRK experience almost the same dispersion, wherein TRKN possesses the minimum numerical dispersion and SPRK shows the largest dispersion. For example, as indicated in figure 1, excepting for the $x$- and $z$-directions, the maximum numerical dispersive errors of the M1, M2, TPRK and TRKN methods are 6%, 5.96%, 5.97% and 5.05%, respectively, while the dispersion error of SPRK is 7.58%, which means that the TRKN scheme can suppress numerical dispersion more efficiently. The dispersion error of SPRK is the largest, while the dispersion errors of M1, M2 and TPRK are situated between those of SPRK and TRKN.

## 4. Numerical verification

In this section, we conduct two numerical experiments to demonstrate the validity of the modified schemes. Due to the restrictions presented by computer storage capacity and computing speed, one may only use a limited model to simulate elastic wave propagation. To avoid spurious reflections from artificial boundaries, a perfectly matched layer (PML) for second-order elastic wave equation are adopted (Komatitsch and Tromp 2003, Liu *et al* 2014b). Correspondingly, in both examples herein, spatial discretization using an eighth-order FD operator was employed.

### *4.1. 2D homogeneous medium*

The first numerical experiment involves a homogeneous velocity model, which is used to test the accuracy and efficiency of the modified schemes. Numerical solutions generated utilizing the modified schemes are compared with analytic solutions, which are obtained using the Cagniard–De Hoop method (De Hoop 1960). The model size is 2000 m × 2000 m. The $P$-wave velocity is $V_P = 2000$, and the $S$-wave velocity is $V_s = 1154.7\ \text{m s}^{-1}$. The mass density is $\rho = 2073\ \text{kg m}^{-3}$. The vertical force, whose time function is a Ricker wavelet with a peak frequency of 25 Hz, is placed at (1000 m, 1000 m). Two receivers, R1 and R2, are located at (1300 m, 800 m) and (1500 m, 800 m), respectively. The spatial sampling interval is 10 m, and the time increment is 0.001 s. The PML with a thickness of 20 grids width surrounds the model.

In figure 2, the waveforms generated by the five methods are compared with the analytical solutions. Figures 2(a) and (b), which demonstrate the curves coincident with the analytic solution, represent the comparisons of the vertical components generated by the five methods with the analytic solution. The curves in figures 2(c) and (d) correspond to the partial magnification of the curves in figures 2(a) and (b), respectively. If we locally magnify figures 2(a) and (b), we can find that SPRK deviated from analytic solution severely.

Compared with figure 2(c), the curves of schemes M1, M2, TPRK, and TRKN in figure 2(d) are not as close to the analytic solution (black curves). With the increase of propagation distance, the accumulated errors of the third-order methods increase, which are still substantially fewer than that of the second-order method. These phenomena can be explained by the numerical dispersion property.

In table 2, we provide a quantitative comparison of the five methods. Because M1 and M2 are derived from SPRK, we normalize the memory cost and CPU time of the five methods to those of SPRK. The memory requirements of the five methods are almost equivalent, though it is worth mentioning that, although the SPRK method requires the least CPU time among the five methods, the error of the SPRK method is the largest. The CPU times of M1 and M2 are less than those of TPRK and TRKN, but the L2 error is almost the same between TPRK and TRKN. As shown in the last line in table 2, a longer travel distance (corresponding to a longer

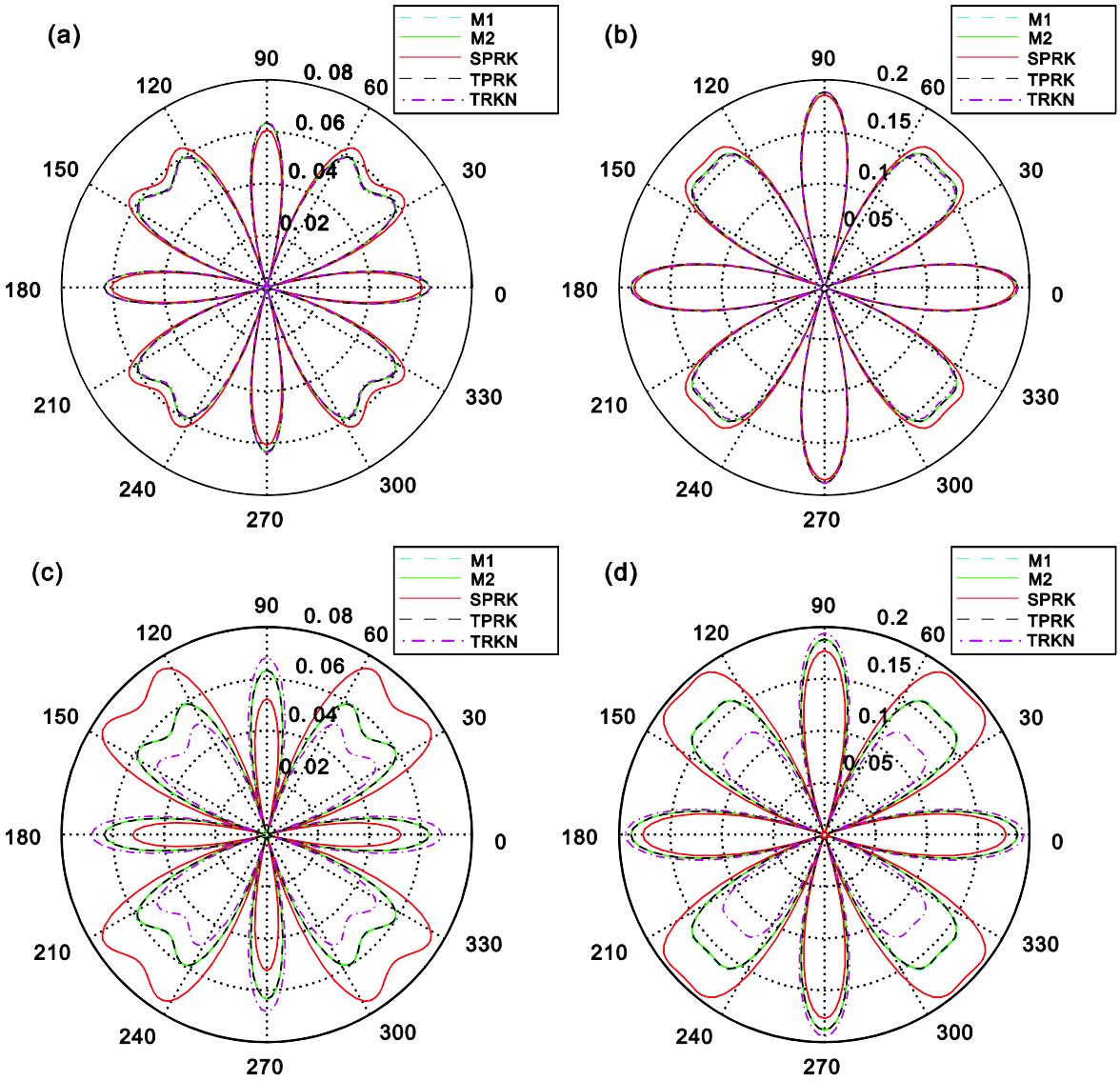


**Figure 1.** Numerical dispersive errors evaluated by |1-R| of five methods. (a) $S_p = 0.4$ and (b) $S_p = 0.5$ with $\alpha = 0.2$; (c) $S_p = 0.4$ and (d) $S_p = 0.5$ with $\alpha = 0.4$.

wave propagation time) results in M2 exhibiting the smallest error among the five methods. Numerical results show that the M2 scheme has improved performance compared with M1 in terms of computational accuracy.

### *4.2. Long-term calculation*

To test the long-term performance of the modified PRK scheme, we now consider a more complex model known as Sigsbee2B (figure 3). In this model, the *P*-wave velocity ranges from 1437 to 4511 m s$^{-1}$, and the *S*-wave velocity is derived using $V_S = V_P/\sqrt{3}$. The mass density is $\rho = 310 \times V_p{}^{0.25}$ (Liu *et al* 2014a). The number of grid points is $300 \times 800$, and the model size is 3000 m $\times$ 8000 m. An explosive source was located at $(x_s, z_s) = (4000\text{ m}, -30\text{ m})$, which is a Ricker wavelet with a frequency of 20 Hz. The spatial increment is 10 m, and the time increment is 0.001 s. Receivers are located on the surface from the leftmost to rightmost of the model with a receiver interval of 10 m. The thickness of PML is 30 grids width.

We compare the schemes M2 and SPRK in this experiment, which are chosen because we have previously proven that M2 possesses the best accuracy after long wave propagation distances while SPRK has the worst, which is apparent in table 2. Because synthetic seismograms generated by M2 (see figure 4(a)) and SPRK (see figure 4(b)) are very similar, we plot the following error of the synthetic seismograms:

$$\mathrm{Csg}D = \mathrm{Csg}S_{\mathrm{norm},\Delta t} - \mathrm{Csg}R_{\mathrm{norm},\Delta t/k} \tag{23}$$

where Csg$D$ denotes the error of the common shot synthetic gathers; Csg$S_{\mathrm{norm},\Delta t}$ are the normalized common shot gathers computed by M2 or SPRK with a time-step of $\Delta t = 0.001$ s;

**Table 2.** Quantitative comparisons of the five methods.

| | Method | | | | |
|---|---|---|---|---|---|
| Parameters | M1 | M2 | SPRK | TPRK | TRKN |
| Memory (KB) | 100.25% | 100.09% | 100% | 100.06% | 100.28% |
| CPU time (s) | 144.24% | 144.52% | 100% | 148.11% | 148.49% |
| Error (R1) | 1.0614 | 1.0567 | 2.8716 | 1.0539 | 1.0636 |
| Error (R2) | 1.5701 | 1.5600 | 3.7272 | 1.5652 | 1.5682 |

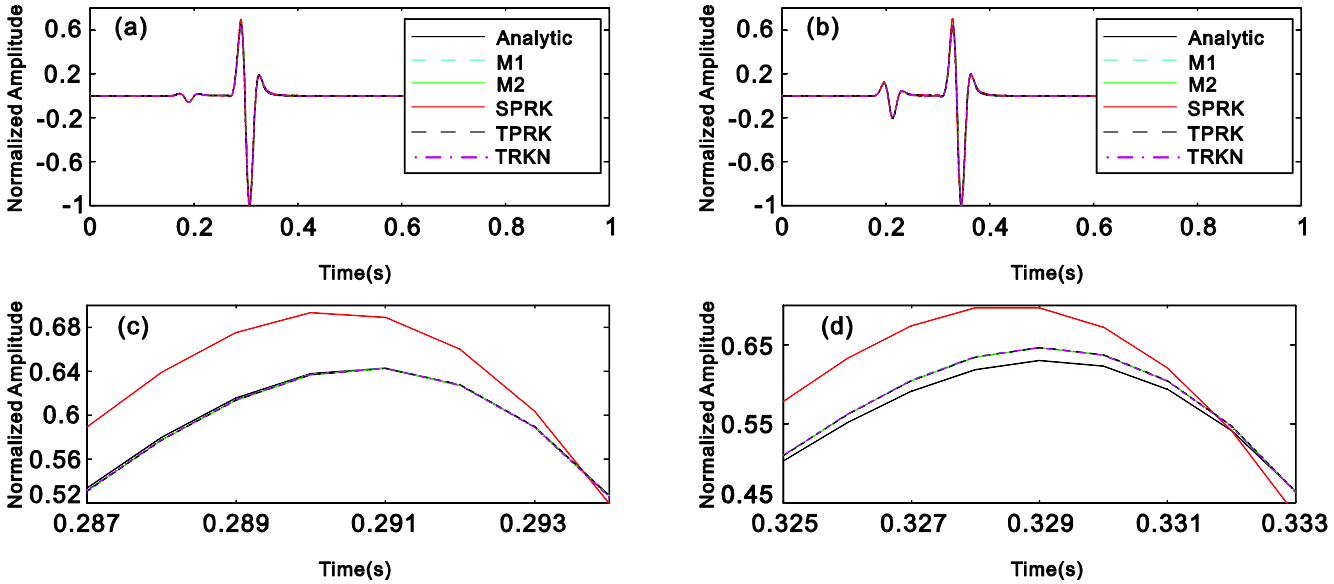


**Figure 2.** Comparison of vertical displacements generated by the five methods with the analytic solution at receivers of R1 (a) and R2 (b). Plots (c) and (d) correspond to the partial magnifications of plots (a) and (b), respectively.

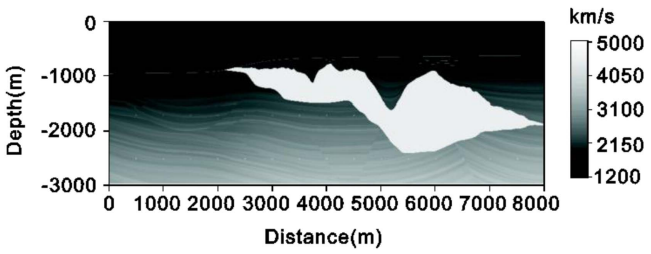


**Figure 3.** Heterogeneous media model: the Sigsbee2B velocity model.

and Csg$R_{\mathrm{norm},\Delta t/k}$ are the normalized reference common shot gathers computed by the method with the best accuracy. A larger $k$ value indicates a more accurate reference result. Here, we select M2 and $k = 2$, and a time-step of $\Delta t/k = 0.0005$ s. The synthetic ground records of the vertical displacement Csg$D$ calculated by method M2 and SPRK are shown in figures 4(c) and (d), respectively.

In figure 4, visual observations demonstrate that the difference between M2 and the reference solution (figure 4(c)) is smaller than the difference between SPRK and the reference solution (figure 4(d)). The maximum relative errors of the M2 and SPRK schemes are 5.73% and 6.79%, respectively, which indicates that synthetic seismology from M2 is more similar to the reference seismology. Thus, it is apparent that M2 can generate reliable results in long-term situations.

## 5. Conclusions

By including an additional spatial operator to the first item or third item of a conventional symplectic scheme, we obtained two new symplectic schemes with third-order accuracy. Generally, a modified strategy of inserting additional high-order spatial operators into the first item of a conventional symplectic scheme is slightly inferior to a scheme wherein additional high-order spatial operators are appended to the third item of a conventional symplectic scheme. Through theoretical analysis and experimental results, we can draw the following conclusions: First, the symplectic condition is automatically satisfied if the order condition holds; second, the two new schemes have properties of low numerical dispersion, strong stability, high accuracy and high efficiency; third, the new numerical schemes can be easily combined with other spatial discretization operators, such as FEM and

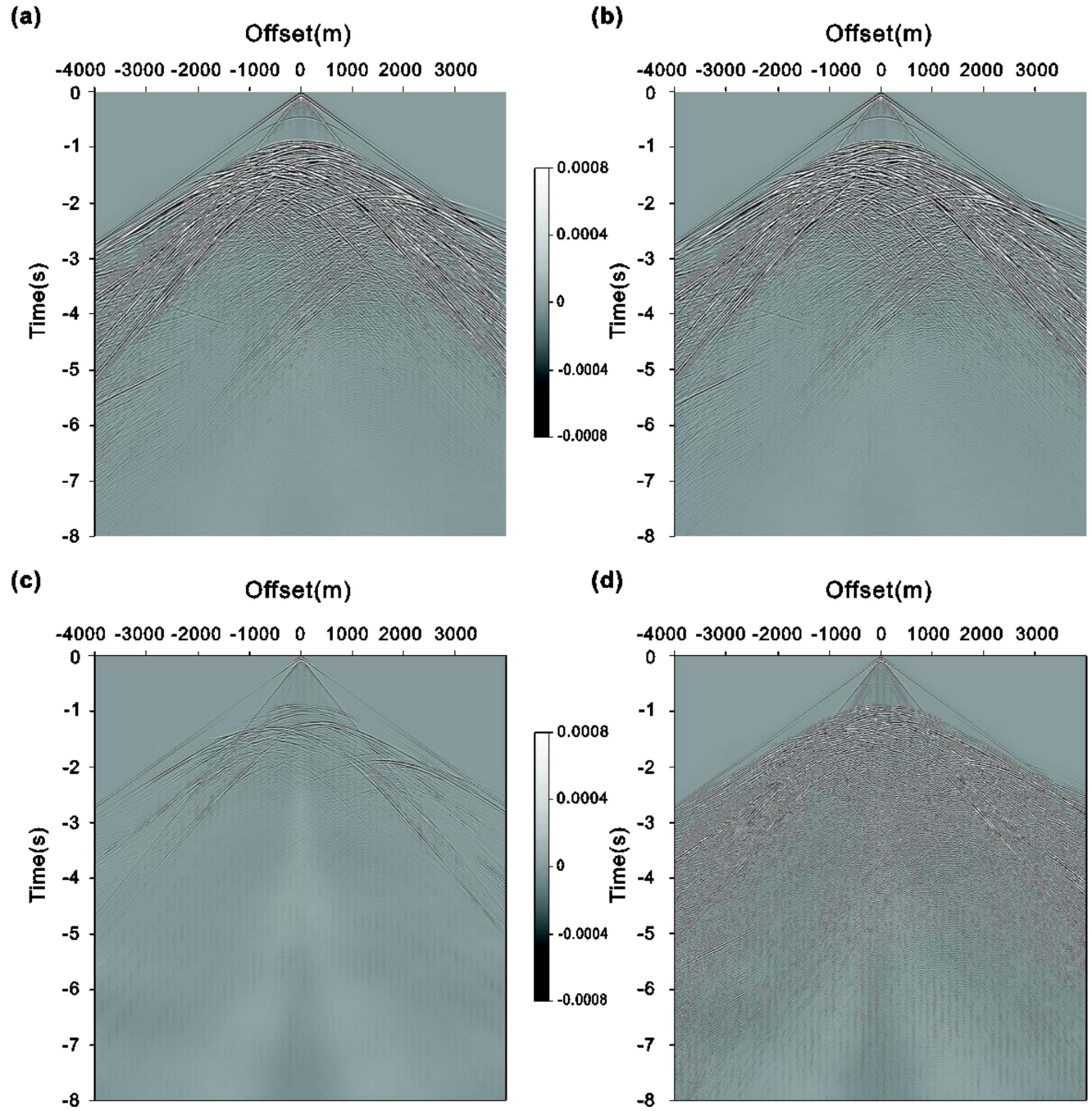


**Figure 4.** Synthetic seismograms generated by M2 (a) and SPRK (b). (c) The error between M2 and the reference solution; (d) the error between SPRK and the reference solution.

SEM. In future work, we will continue to explore the broad applications of this modified strategy.

## Acknowledgments

We thank Shaolin Liu for providing the C code for synthetic examples. The suggestions from Shaolin Liu are greatly acknowledged. This study was supported by the National Natural Science Foundation of China (Grant No. 41604034).

## Appendix A

The symplectic conditions of M1 and M2 are described herein. From equation (8), the values of $U^{n+1}$ and $V^{n+1}$ are as follows:

$$\begin{cases} V^{n+1} = V^n + (b_1 + b_2)\Delta t L U^n + (b_1 B_1 + b_2(B_1 \\ \quad + B_2))\Delta t^2 L V^n + b_1 b_2 B_2 \Delta t^3 L^2 U^n \\ \quad + (b_1 B_3 + b_2(B_3 + b_1 B_1 B_2))\Delta t^4 L^2 V^n \\ \quad + b_1 b_2 B_2 B_3 \Delta t^6 L^3 V^n \\ U^{n+1} = U^n + (B_1 + B_2)\Delta t V^n + b_1 B_2 \Delta t^2 L U^n \\ \quad + (B_3 + b_1 B_1 B_2)\Delta t^3 L V^n + b_1 B_2 B_3 \Delta t^5 L^2 V^n \end{cases} . \quad \text{(A1)}$$

The corresponding Taylor series expansions of $V^{n+1}$ and $U^{n+1}$ are:

$$\begin{cases} V^{n+1} &= V^n + \Delta t L U^n + \frac{1}{2}\Delta t^2 L V^n + \frac{1}{6}\Delta t^3 L^2 U^n \\ & \quad + o(\Delta t^4) \\ U^{n+1} &= U^n + \Delta t V^n + \frac{1}{2}\Delta t^2 L U^n + \frac{1}{6}\Delta t^3 L V^n \\ & \quad + o(\Delta t^4) \end{cases}. \tag{A2}$$

By comparing the coefficients of systems (A1) and (A2), we obtain

$$\begin{cases} b_1 + b_2 = 1 \\ B_1 + B_2 = 1 \\ b_2 + b_1 B_1 = \frac{1}{2} \\ b_1 b_2 B_2 = \frac{1}{6} \\ b_1 B_1 B_2 + B_3 = \frac{1}{6} \end{cases}. \tag{A3}$$

The solution of (A3) is as follows:

$$b_1 = \frac{2}{3}, \quad b_2 = \frac{1}{3}, \quad B_1 = \frac{1}{4}, \quad B_2 = \frac{3}{4}, \quad B_3 = \frac{1}{24}. \tag{A4}$$

From equation (11), we can get:

$$\begin{cases} V^{n+1} &= V^n + (b_1 + b_2)\Delta t L U^n + ((B_1 + B_2) b_2 \\ & \quad + B_1 b_1)\Delta t^2 L V^n + B_2 b_1 b_2 \Delta t^3 L^2 U^n \\ & \quad + (B_1 B_2 b_1 + B_3) b_2 \Delta t^4 L^2 V^n + B_3 b_1 b_2 \\ & \quad \times \Delta t^5 L^3 U^n + B_1 B_3 b_1 b_2 \Delta t^6 L^3 V^n \\ U^{n+1} &= U^n + (B_1 + B_2)\Delta t V^n + B_2 b_1 \Delta t^2 L U^n \\ & \quad + (B_1 B_2 b_1 + B_3)\Delta t^3 L V^n + B_3 b_1 \Delta t^4 L^2 \\ & \quad \times U^n + B_3 B_1 b_1 \Delta t^5 L^2 V^n \end{cases}. \tag{A5}$$

By comparing the coefficients of equations (A5) and (A2), we obtain

$$\begin{cases} b_1 + b_2 = 1 \\ B_1 + B_2 = 1 \\ b_2 + B_1 b_1 = \frac{1}{2} \\ B_2 b_1 b_2 = \frac{1}{6} \\ B_1 B_2 b_1 + B_3 = \frac{1}{6} \end{cases}. \tag{A6}$$

We can observe from equations (A3) and (A6) that schemes M1 and M2 have the same coefficients.

## Appendix B

From equation (8) and condition (10), $V$ and $U$ at $n + 1$ time steps can be written as

$$\begin{bmatrix} V^{n+1} \\ U^{n+1} \end{bmatrix} = \begin{bmatrix} A_{11} & A_{12} \\ A_{21} & A_{22} \end{bmatrix} \begin{bmatrix} V^n \\ U^n \end{bmatrix}, \tag{B1}$$

where $a_{11}$, $a_{12}$, $a_{21}$ and $a_{22}$ are defined by the five variables of equation (10), which can be written as

$$\begin{cases} A_{11} = I_3 + \frac{1}{2}\Delta t^2 L + \frac{1}{12}\Delta t^4 L^2 + \frac{1}{144}\Delta t^6 L^3 \\ A_{12} = \Delta t L + \frac{1}{6}\Delta t^3 L^2 \\ A_{21} = \Delta t I_3 + \frac{1}{6}\Delta t^3 L + \frac{1}{48}\Delta t^5 L^2 \\ A_{22} = I_3 + \frac{1}{2}\Delta t^2 L \end{cases}, \tag{B2}$$

where $I_3$ is a $3 \times 3$ identity matrix. The symplectic condition of equation (5) can be written in an equivalent form (Hairer *et al* 2006):

$$A^T J A = J, \tag{B3}$$

where $A$ is the transformation matrix of equation (B1), and $J$ is the skew-symmetric matrix. To hold (B3) true, the spatial operator $L$ should be symmetric (see appendix C):

$$J = \begin{bmatrix} 0 & I_3 \\ -I_3 & 0 \end{bmatrix}. \tag{B4}$$

From (B3) and (B4), the symplectic condition obeys the following equation:

$$A_{11} A_{22} - A_{12} A_{21} = I_3. \tag{B5}$$

Substituting (B2) into (B5), we can find that (B5) holds, which means that the symplectic condition of M1 holds. Using the same process, we can find that the symplectic condition of M2 also holds.

## Appendix C

The 1D elastic wave within a homogeneous media is considered. The only displacement component $u = u_1$ is simply a function of the coordinates $x = x_1$ and time $t$. The wave equation can be simplified as

$$\frac{\partial^2 u(x, t)}{\partial x^2} = \frac{1}{c^2}\ddot{u}(x, t), \tag{C1}$$

where $c$ is the wave velocity, i.e., for a $p$-wave, $c = \sqrt{\frac{\lambda + 2\mu}{\rho}}$, and for an $s$-wave, $c = \sqrt{\frac{\mu}{\rho}}$.

Let $H(u, v) = \frac{1}{2}\int (v^2 + u_x^2)\mathrm{d}x$, following which the Hamiltonian system is

$$\frac{\mathrm{d}z}{\mathrm{d}t} = J^{-1}H_z, \tag{C2}$$

where $z = \begin{bmatrix} v \\ u \end{bmatrix}$, $J^{-1} = \begin{bmatrix} 0 & -1 \\ 1 & 0 \end{bmatrix}$, $H_z = \begin{bmatrix} \frac{\delta H}{\delta v} \\ \frac{\delta H}{\delta u} \end{bmatrix} = \begin{bmatrix} v \\ -u_{xx} \end{bmatrix}$. (C2) can then be written as $\frac{\mathrm{d}z}{\mathrm{d}t} = J^{-1}Az$, where $J^{-1}A = \begin{bmatrix} 0 & \Delta \\ 1 & 0 \end{bmatrix}$, and where $\Delta$ denotes the $2N$ order FD spatial operator of $\frac{\partial^2}{\partial x^2}$, which is based on the Taylor series expansion

$$\frac{\partial^2 u_m}{\partial x^2} = \sum_{k=-N}^{N} \frac{c_k u(m+k)}{\Delta x^2}, \tag{C3}$$

where $m$ denotes the number of FD nodes, and $c_k$ is the coefficient of the FD series expansion: $c_0 = -2\sum_{k=1}^{N} c_k$, $c_k = c_{-k}$, $k = 1, 2, \cdots, N$.

When $N = 1$, $c_{-1} = 1$, $c_0 = -2$, $c_1 = 1$.

When $N = 2$, $c_{-2} = -\frac{1}{12}$, $c_{-1} = \frac{4}{3}$, $c_0 = -\frac{5}{2}$, $c_1 = \frac{4}{3}$, $c_2 = -\frac{1}{12}$.

When $N > 2$,

$$c_k = \frac{(-1)^{k+1}}{k^2} \frac{\prod_{i=1, i\neq k}^{N} i^2}{\prod_{i=1}^{k-1}(k^2 - i^2)\prod_{i=k+1}^{N}(i^2 - k^2)} \quad (k = 1, 2, \cdots, N). \tag{C4}$$

Let $U = [u(1), u(2), \cdots u(n)]'$, $V = [v(1), v(2), \cdots v(n)]'$, and then (C2) can be written as

$$\frac{\mathrm{d}}{\mathrm{d}t}\begin{bmatrix} V \\ U \end{bmatrix} = \begin{bmatrix} & L \\ I & \end{bmatrix}\begin{bmatrix} V \\ U \end{bmatrix} = \begin{bmatrix} LU \\ V \end{bmatrix}. \tag{C5}$$

Considering the symmetry of the coefficients $c_k = c_{-k}$ and the periodicity of the boundary conditions, $L$ is symmetry, for example:

when $N = 1$, $L$ is

$$L: \frac{1}{\Delta x^2}\begin{bmatrix} -2 & 1 & 0 & \cdots & \cdots & 1 \\ 1 & -2 & 1 & \cdots & \cdots & 0 \\ & \ddots & \ddots & \ddots & & \\ & \ddots & \ddots & \ddots & & \\ 0 & 0 & \cdots & \cdots & -2 & 1 \\ 1 & 0 & \cdots & \cdots & 1 & -2 \end{bmatrix}, \tag{C6}$$

when $N = 2$, $L$ is

$$L: \frac{1}{12\Delta x^2}\begin{bmatrix} -30 & 16 & -1 & 0 & 0 & \cdots & \cdots & 0 & -1 & 16 \\ 16 & -30 & 16 & -1 & 0 & \cdots & \cdots & 0 & 0 & -1 \\ & \ddots & \ddots & \ddots & \ddots & \ddots & & & & \\ & & \ddots & \ddots & \ddots & \ddots & \ddots & & & \\ & & & \ddots & \ddots & \ddots & \ddots & \ddots & & \\ & & & & \ddots & \ddots & \ddots & \ddots & \ddots & \\ & & & & & \ddots & \ddots & \ddots & \ddots & \ddots \\ & & & & & & \ddots & \ddots & \ddots & \ddots \\ -1 & 0 & 0 & \cdots & \cdots & \cdots & \cdots & 16 & -30 & 16 \\ 16 & -1 & 0 & \cdots & \cdots & \cdots & \cdots & -1 & 16 & -30 \end{bmatrix}. \tag{C7}$$

## References


Aki K and Richards P 1980 *Quantitative Seismology* (New York: W H Freeman)

Alford R M, Kelly K R and Boore D M 1974 Accuracy of finite-difference modeling of the acoustic wave equation *Geophysics* **39** 834–42

Chen J B 2007 High-order time discretizations in seismic modeling *Geophysics* **72** SM115–22

Chen J B 2009 Lax–Wendroff and Nyström methods for seismic modelling *Geophys. Prospect.* **57** 931–41

Dablain M A 1986 The application of high-differencing to the scalar wave equation *Geophysics* **51** 54–66

De Basabe J D and Sen M K 2007 Grid dispersion and stability criteria of some common finite-element methods for acoustic and elastic wave equations *Geophysics* **72** T81–95

De Basabe J D and Sen M K 2010 Stability of high-order finite elements for acoustic and elastic wave propagation with high-order time stepping *Geophy. J. Int.* **181** 577–90

De Hoop A T 1960 A modification of Cagniard's method for solving seismic pulse problems *Appl. Sci. Res.* **8** 349–56

Feng K and Qin M Z 2010 *Symplectic Geometric Algorithms for Hamiltonian Systems* (Berlin: Springer)

Hairer E, Lubich C and Wanner G 2006 *Geometric Numerical Integration: Structure-Preserving Algorithms for Ordinary Differential Equations* (Berlin: Springer)

Iwatsu R 2009 Two new solutions to the third-order symplectic integration method *Phys. Lett.* A **373** 3056–60

Komatitsch D and Tromp J 2003 A perfectly matched layer absorbing boundary condition for the second-order seismic wave equation *Geophys. J. Int.* **154** 146–53

Komatitsch D and Vilotte J P 1998 The spectral element method: an efficient tool to simulate the seismic response of 2D and 3D geological structures *Bull. Seismol. Soc. Am.* **88** 368–92

Kosloff D D and Baysal E 1982 Forward modeling by a Fourier method *Geophys.* **7** 1402–12

Li X F, Li Y Q, Zhang M G and Zhu T 2011 Scalar seismic-wave equation modeling by a multisymplectic discrete singular convolution differentiator method *Bull. Seismol. Soc. Am.* **101** 1710–8

Li X F, Wang W S, Lu M W, Zhang M G and Li Y Q 2012 Structure-preserving modelling of elastic waves: a symplectic discrete singular convolution differentiator method *Geophys. J. Int.* **188** 1382–92

Liu S L, Li X F, Wang W S, Liu Y S, Zhang M G and Zhang H 2014a A new kind of optimal second-order symplectic scheme for seismic wave simulations *Sci. China Earth. Sci.* **57** 751–8

Liu S L, Li X F, Wang W S and Liu Y S 2014b A mixed-grid finite element method with PML absorbing boundary conditions for seismic wave modelling *J. Geophys. Eng.* **11** 055009

Liu S L, Li X F, Wang W S, Xu L and Li B F 2015a A modified symplectic scheme for seismic wave modeling *J. Appl. Geophys.* **116** 110–20

Liu S L, Li X F, Wang W S and Zhu T 2015b A symplectic RKN scheme for solving elastic wave equations *Chin. J. Geophys.* **58** 1355–66 (in Chinese)

Liu S L, Li X F, Wang W S and Zhu T 2015c Source wavefield reconstruction using a linear combination of the boundary wavefield in reverse time migration *Geophysics* **80** s203–12

Liu S L, Yang D H, Lang C, Wang W S and Pan Z D 2017a Modified symplectic nearly-analytic discrete methods for acoustic wave simulations *Comput. Phys. Commun.* **213** 52–63

Liu S L, Yang D H and Ma J 2017b A modified symplectic PRK scheme for seismic wave modeling *Comput. Geosci.* **99** 28–36

Ma X, Yang D H, Song G J and Wang M X 2014 A low-dispersive symplectic partitioned Runge–Kutta method for solving seismic-wave equations: I. Scheme and theoretical analysis *Bull. Seismol. Soc. Am.* **104** 2206–25

Marfurt K J 1984 Accuracy of finite-difference and finite-element modeling of the scalar and elastic wave equations *Geophysics* **49** 533–49

Mclachlan R I and Atela P 1992 The accuracy of symplectic integrators *Nonlinearity* **5** 541–62

Moczo P 1989 Finite-difference technique for SH -waves in 2D media using irregular grids-application to the seismic response problem *Geophys. J. Int.* **99** 321–9

Moczo P, Kristek J and Halada L 2000 3D fourth-order staggered-grid finite-difference schemes: stability and grid dispersion *Bull. Seismol. Soc. Am.* **90** 587–603

Okunbor D and Skeel R D 1992 Explicit canonical methods for Hamiltonian systems *Math. Comput.* **59** 439–55

Okunbor D I and Skeel R D 1994 Canonical Runge–Kutta–Nyström methods of orders five and six *J. Comput. Appl. Math.* **51** 375–82

Patera A T 1984 A spectral element method for fluid dynamics: laminar flow in a channel expansion *J. Comput. Phys.* **54** 468–88

Sun G 1993 Symplectic partitioned Runge–Kutta methods *J. Comput. Math.* **11** 365–72

Virieux J 1984 SH-wave propagation in heterogeneous media: velocity-stress finite-difference method *Geophysics* **49** 1933–42

Virieux J 1986 P-SV wave propagation in heterogeneous media: velocity-stress finite-difference method *Geophysics* **51** 889–901

Wang M and Xu S 2015 Finite-difference time dispersion transforms for wave propagation *Geophysics* **80** WD19–25

Whitmore N and Lines L R 1986 Vertical seismic profiling depth migration of a salt dome flank *Geophysics* **51** 1087–1109

Yang D H 2006 Optimal nearly analytic discrete approximation to the scalar wave equation *Bull. Seismol. Soc. Am.* **96** 1114–30

Yang D H, Song G J and Lu M 2007 Optimally accurate nearly analytic discrete scheme for wave-field simulation in 3D anisotropic media *Bull. Seismol. Soc. Am.* **97** 1557–69

Yang D H, Teng J W, Zhang Z J and Liu E R 2003 A nearly analytic discrete method for acoustic and elastic wave equations in anisotropic media *Bull. Seismol. Soc. Am.* **93** 882–90